

Acoustic Phased Array Quantification of Quiet Technology Demonstrator 3 Advanced Inlet Liner Noise Component

Leon Brusniak¹, Jackie W. Wong² and Eric H. Nesbitt³
The Boeing Company, Seattle, WA, 98124, USA

Michael G. Jones⁴ and Douglas M. Nark⁵
NASA Langley Research Center, Hampton, VA, 23681, USA

Acoustic phased array flyover noise measurements were acquired as part of the Boeing 737 MAX-7 NASA Advanced Inlet Liner segment of the Quiet Technology Demonstrator 3 (QTD3) flight test program. This paper reports on the processes used for separating and quantifying the engine inlet, exhaust and airframe noise source components and provides sample phased array-based comparisons of the component noise source levels associated with the inlet liner treatment configurations.

I. Nomenclature

a, b, \dots, k	=	phased array subarray identifiers
BPF	=	blade passage frequency
CBF	=	Conventional Beamforming
DAMAS2	=	Deconvolution Approach for the Measurement of Acoustics Sources 2
NASA	=	National Aeronautics and Space Administration
QTD3	=	Quiet Technology Demonstrator 3
ϕ	=	angle relative to overhead at phased array center

II. Introduction

Full scale flyover noise testing of NASA advanced inlet liners was conducted as part of the Quiet Technology Demonstrator 3 flight test program in July and August of 2018. Details on the inlet designs and testing are provided in the companion paper of Reference 1. The present paper provides supplemental details relating to the acoustic phased array portion of the analyses provided in Ref. 1. In brief, the test article was a Boeing 737MAX-7 aircraft with a modified right hand (starboard side) engine inlet, which consisted of either a production inlet liner, a NASA designed inlet liner or a simulated hard wall configuration (accomplished by applying speed tape over the inlet acoustic treatment areas). In all three configurations, the engine forward fan case acoustic panel was replaced with a unperforated (hardwall) panel. No other modifications to any other acoustic treatment areas were made. The left hand (port side) engine was a production engine and was flown at idle thrust for all measurements in order to isolate the effects of the inlet liners to the right hand engine. As described in Ref. 1, the NASA inlet treatment consists of laterally cut slots (cut perpendicular to the flow direction) which are designed to reduce excrescence drag while maintaining or exceeding the liner acoustic noise reduction capabilities. The NASA inlet liner consists of a Multi-Degree of Freedom (MDOF) design with two breathable septum layers inserted into each honeycomb cell [1]. The aircraft noise

¹ Product Development Community Noise.

² Principal Investigator, Product Development Community Noise.

³ Technical Fellow, Product Development Community Noise, Senior Member AIAA.

⁴ Technical Point of Contact Engineer, Structural Acoustics Branch, Associate Fellow AIAA.

⁵ Engineer, Structural Acoustics Branch, Associate Fellow AIAA.

The material is based upon work supported by the National Aeronautics and Space Administration under Contract Number NNL16AA04B. Any opinions, findings, and conclusions or recommendations expressed in this material are those of the author(s) and do not necessarily reflect the views of the National Aeronautics and Space Administration.

measurements were acquired for both takeoff (flaps 1 setting, gear up) and approach (flaps 30 gear up and gear down) configurations. The inlet and flight test configurations are summarized in Table 1.

Table 1: Inlet Treatment and Flight Configurations

Inlet	Forward Fan Case	Aircraft
Production	Hardwall	Flaps 1, gear up; flaps 30 gear up; flaps 30 gear down
NASA	Hardwall	Flaps 1, gear up; flaps 30 gear up; flaps 30 gear down
Hardwall	Hardwall	Flaps 1, gear up; flaps 30 gear up; flaps 30 gear down

III. Test Description and Hardware

The flight testing was conducted at the Grant County airport in Moses Lake, WA, between 27 July and 6 August 2018. The noise measurement instrumentation included 8 flush dish microphones arranged in a noise certification configuration as well as an 840 microphone phased array. The flush dish microphones were used to quantify the levels and differences in levels between the various inlet treatments. The phased array was used to separate and quantify the narrowband (tonal) and broadband noise component levels from the engine inlet/exhaust and from the airframe. Phased array extraction of the broadband component was critical to this study because it allowed for the separation of the inlet component from the total airplane level noise even when it was significantly below the total level. Figure 1 provides an overview of the phased array microphone layout as well as a detailed image of an individual phased array microphone mounted in a plate holder (the microphone sensor is the dot in the center of the plate). The ground plane ensemble array microphones (referred to as “ensemble array” in this paper) were mounted in plates with “flower petal” edges designed to minimize edge scattering effects.



Fig. 1 Flyover test microphone layout.

The phased array configuration was the result of a progressive development of concepts originally implemented in Ref. 2 and refined over the following years, consisting namely of multiple multi-arm logarithmic spiral subarrays designed to cover overlapping frequency ranges and optimized for various aircraft emission angles. For the present case, the signals from all 840 microphones were acquired on a single system. The 840 microphones were parsed into 11 primary subarray sets spanning from smallest to largest aperture size and labeled accordingly as “ a, b, \dots, k ”, where “ a ” corresponds to the smallest fielded subarray and “ k ” corresponds to the largest aperture subarray. The apertures ranged from approximately 10 ft to 427 ft in size (in the flight direction) with the subarrays consisting of between 215

and 312 microphones. Figure 2 shows three such subarrays, k , h and a . As done in Ref. 2, microphones were shared between subarrays in order to reduce total channel count.

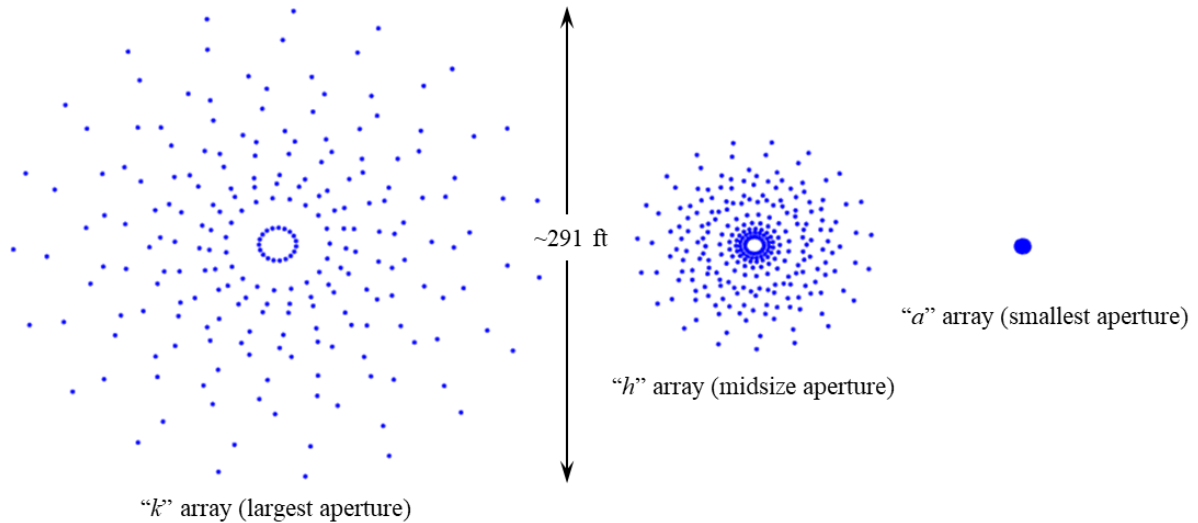


Fig. 2 Sample subarray sizes (20° from overhead – refer to Figure 3a discussion).

In addition to the above, each of the 11 primary subarray sets consisted of four subarrays optimized to provide near equivalent array spatial resolution in both the flight and lateral directions within 30 degrees of overhead (i.e., airplane directly above the center of the array), namely, at angles ϕ of 0, ± 10 , ± 20 and ± 30 degrees relative to overhead where angle ϕ is defined as shown in Figure 3a. This allowed for optimized aircraft noise measurements from 60 to 120 degree emission angle.⁶ An example of this pletharray design is shown in Figure 3b for the k subarray. When the aircraft is at overhead, the microphones indicated by the blue markers are used for beamforming. When the aircraft is at angles ± 10 degrees from overhead, both the blue and red colored microphones are used, and so on for the ± 20 and ± 30 degree aircraft locations. See Ref. 3 for extensive details on pletharray design for aeroacoustic phased array testing.

⁶ In the discussions that follow, emission angle values are used. These are the angles at the time sound is emitted relative to the engine axis and are calculated based on flight path angle, body aircraft body angle with respect to the relative wind direction, and engine axis angle relative to aircraft body angle.

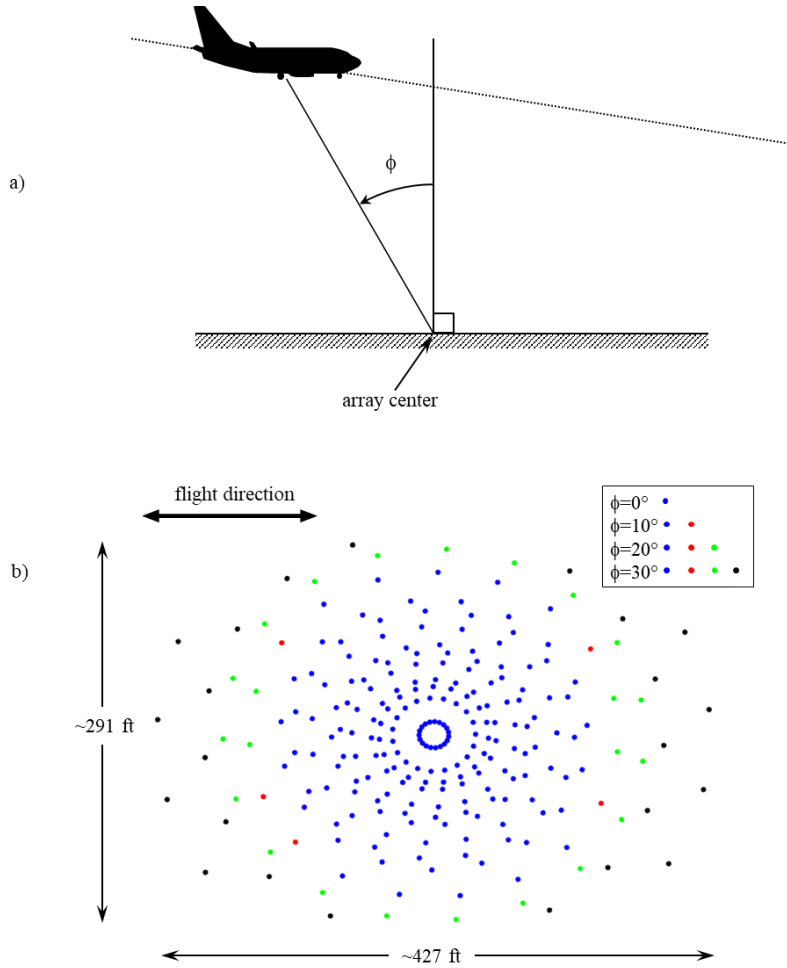


Fig. 3 Array geometry definitions a) reference array design point angle ϕ , b) k subarray microphone element selection versus ϕ ($\phi=30$ degree case shown; $\phi=0$ is aircraft overhead at array center).

IV. Phased Array Processing

This section describes a Boeing process for quantifying aircraft noise subcomponent levels using flyover phased array data. The phased array noise decomposition process utilized traditional time domain beamforming (known as delay-and-sum, or Conventional Beamforming (CBF)) with Doppler shifts removed from the data as per the methods of Ref. 4. The narrowband CBF noise source maps were then deconvolved using the DAMAS2 algorithm of Ref. 5. See also Reference 6 which provides a validation study on the use of the DAMAS2 algorithm for flyover phased array applications. Array shading was not utilized in this study.

In order to conduct meaningful data analyses, the frequencies over which the various phased array subarrays provide the best response must be quantified. Historical efforts for identifying the usable frequency ranges have relied on qualitative visual examinations of the character of each beamform map to estimate the lowest frequency at which a given subarray becomes effective in localizing noise sources, and to also estimate the highest frequencies at which the array still provides meaningful information. Such approaches are highly subjective and tedious. Sample beamform map characteristics are illustrated in Figure 4 for a low power takeoff at 80 degree emission angle using the NASA treated inlet. Figure 4b is an example of a clean beamform map from the k array at 488 Hz, with well-defined noise sources (from the right hand engine and inboard leading edge sources). At 73 Hz, Figure 4a, the k array does not have sufficient capability to resolve noise sources. At the higher end of the frequency spectrum (2 kHz), Figure 4c illustrates how de-correlation effects and array side lobes can negatively impact beamform map quality. See Ref. 7 for a discussion of the de-correlation effects due to atmospheric turbulence and other weather related issues.

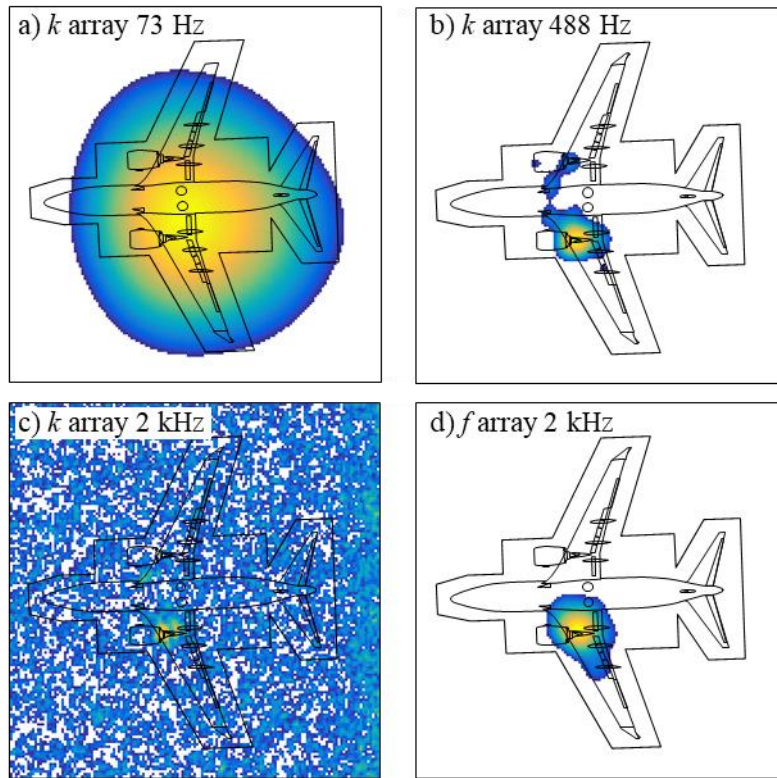


Fig. 4 Beamform map characteristics

The primary characteristics of high quality beamform maps are that all aircraft related noise sources are clearly defined, are associated with known source mechanisms, and do not exhibit spurious side lobes, as exemplified by Figure 4c. This suggests the use of a bounding envelope surrounding the aircraft as shown in each of the four samples in Figure 4. This envelope divides the beamform map into regions internal and external to the envelope with the outer region (the beamforming grid edges) being indicated by the outer black boxes. For a given beamform map, the location of all noise sources within the phased array measurement dynamic range are identified (for example, within 10 dB down from the peak map level and over the entire beamforming grid). Then, the fraction of all of these identified locations that fall within the interior envelope are determined. The red curve in Figure 5a shows the result of such a calculation over all processed frequencies. For Figure 4b, all noise sources fall within the envelope, hence, it receives a scoring value of 1.0 at 488 Hz in Figure 5a (indicated by the upper circular marker). At 73 Hz (Figure 4a), the array is unable to resolve the noise sources, resulting in a large number of beamform map values falling outside of the bounding envelope, hence providing a scoring value of 0.62 in Figure 5a. Similarly, at 2 kHz (Figure 4c), the array is negatively impacted by de-correlation effects, resulting in a low scoring value of 0.30 in Figure 5a (the lower circular marker at this frequency). Examination of the metric scoring values over the entire frequency range in Figure 5a demonstrates that for this particular flyover condition and emission angle, the k subarray is able to provide high quality noise source resolution from approximately 268 Hz to 878 Hz. Further non-subjective quantification of the map quality can be made by selecting only those frequencies for which the metric scoring values exceed a user-selected threshold, for example, 0.98 (as suggested by the horizontal dashed line in Figure 5a). Note that, the higher the threshold value, the fewer the number of frequency bins which may be selected, and conversely, the lower the threshold, the larger the number of selected frequency bins allowed, but at a potential cost of an increased number of lower quality beamform maps.

This approach is further extended to the other available subarrays. As seen, the f subarray is able to cleanly resolve the noise sources at 2 kHz in Figure 4d as compared to the k subarray map at the same frequency in Figure 4c. The green curve in Figure 5a shows the metric values distribution for the f subarray. At 2 kHz, the f subarray has a metric scoring value of 1.0. If these were the only two subarrays available, the two curves in Figure 5a would suggest the

composite use of the k subarray up to approximately 1 kHz and the f subarray above 1 kHz. In the present study, 11 subarrays were available for use. Figure 5b shows the composite result of application of the selection process based on the use of all available subarrays, where the blue and green line colors are used to aid in distinguishing in the image between adjacent selected subarrays. The method is automated (starting with the k subarray) to identify the lowest frequency at which each subarray exceeds the user-specified metric value threshold and to continue using this subarray until the subarray metric values fall below the threshold, at which the next subarray satisfying the threshold value is used. In some instances, none of the subarrays have metric values exceeding the threshold value. In this case, the subarray having the highest average metric values over the given frequency band is used. This effect is seen at the highest end of the spectrum for the b subarray, where metric values as low as 0.8 arise. Note that the a and c subarrays were not selected in this example because, in the process of sweeping from largest to smallest subarrays, the d subarray metric was determined by the automated process to be higher than for the c subarray up to the beginning of the b subarray band shown in Figure 5. Similarly, the b subarray metric value was quantified as being higher than for the a subarray up to the highest frequency shown. Overall, this composite method approach provides optimal, automated and, importantly, non-subjective measures of subarray beamform map quality. A key part of the automation process is that, since the CBF output data are narrowband, the frequency ranges spanned by each subarray in Figure 5b are matched to edges of the corresponding 1/3 octave band frequency edges. That is, the dashed vertical lines in Figure 5b correspond to 1/3 octave band frequency edges. This assures that any array processing effects – such as differences in level at the same frequency for different subarrays – do not spill across the 1/3 octave band frequency edges, which is important for the phased array 1/3 octave band data adjustments described later. Note also that the addition or removal of Doppler shifting effects must be accounted for in the process as needed.

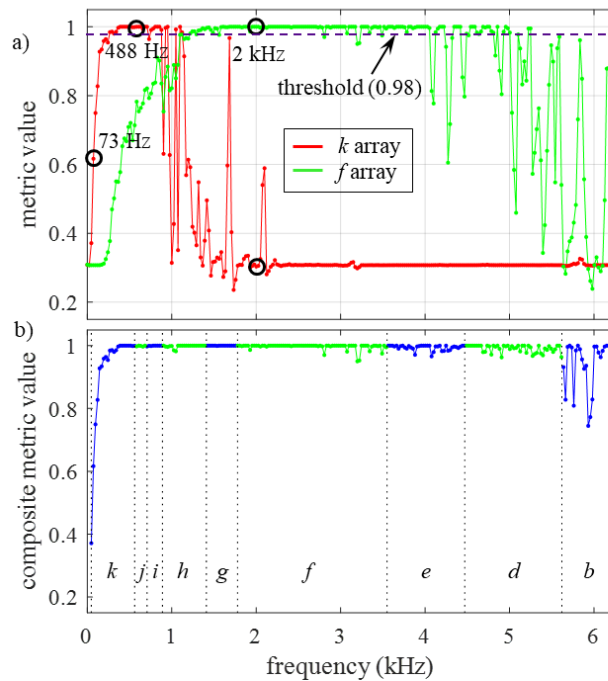


Fig. 5 Phased array data quality scoring metric examples a) sample metric distributions, b) composite metric distribution.

After the composite metric values have been determined for a given subarray, the corresponding data from the deconvolved (DAMAS2) maps are extracted according to the composite metric value mappings (mapping from subarrays to frequency bands).⁷ The deconvolved levels within the beamform map bounding interior envelope are then summed together to produce total aircraft noise levels as measured by and received at the phased array. Such a

⁷ Note that the deconvolved maps could similarly be used for determining composite metric values as was done for Figure 5b using CBF beamform maps.

spectrum is suggested by the red curve in the conceptual illustration in Figure 6 (broadband components, where tones have been removed, as required for the analyses in Ref. 1). The red '+' marks highlight the deconvolved 1/3 octave band data center frequencies, particularly their locations relative to the partial 1/3 octave band edges indicated by the dashed vertical lines in the figure. The subarray/frequency band mapping used is suggested in the figure by the corresponding subarray letter identifiers.

One approach to correcting the deconvolved data to absolute levels would be to account for effects such as spherical spreading, aircraft velocity differences, pressure doubling and atmospheric absorption. However, array processing effects can add uncertainty to the absolute level values. Therefore, an alternate approach was used in which the deconvolved data were frequency matched to the calibrated ensemble array microphone spectra at the corresponding emission angles. This is indicated in Figure 6, where the blue curve corresponds to data from the calibrated ensemble array microphones. To account for array processing effects, the phased array levels at each 1/3 octave frequency are offset to match the ensemble array microphone levels, as exemplified by the direction and magnitude of the sample arrows near both ends of the spectra. The black curve plotted at the top represents the difference in levels between the ensemble array microphones and the phased array total levels. The difference curve values are added to the phased array levels to produce both calibrated phased array total levels and – of key importance to this study – calibrated phased array noise source subcomponent levels.

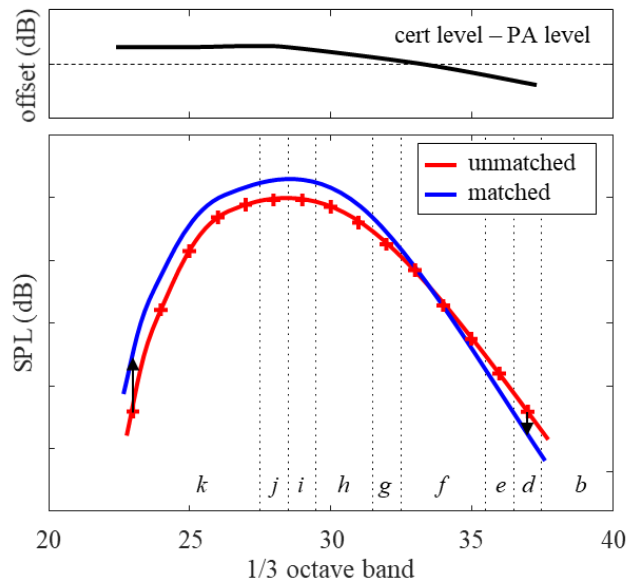


Fig. 6 Conceptual illustration of matching of phased array total levels to ensemble array microphone data.

Note from Figure 1 that the ensemble array microphones and phased array center are not co-located, therefore, the corresponding emission angles between the two locations occur at different times, between which the aircraft could potentially change orientation and hence change noise source directivity.⁸ Prior experience with flyover data which has been accepted as “good” (which is indicated by a small amount of scatter between the individual microphones in the ensemble array) have shown acceptable levels of repeatability for noise subcomponents, so this is not regarded as a likely significant source of data variability. Such assumptions can always be checked by comparing the aircraft performance parameters (velocity, flight trajectory) as it flies over one set of microphones and then the other. An underlying point is that this data matching approach makes use of the measured relative noise source levels within each phased array map (i.e., the component level of one source versus that of another). Reference 8 provides additional information on the phased array noise source decomposition process.

⁸ The ensemble array microphone distribution shown in Figure 1 was actually replicated during the test by the inclusion of additional microphones within the phased array microphone footprint, with the intent of removing any such potential directivity measurement differences. These data were not utilized in this study.

The next step in the analysis process is to identify the regions over which noise subcomponent data are required. As shown in Figure 7, the aircraft was subdivided into a large number of defined noise integration subregions. The airframe noise components are captured by zones 1, 2, 3, 8, 9, 12, 13, 14 and 15. The engine noise components are captured by zones 4, 6, 8 and 10 for the right hand engine and by zones 5, 7, 9 and 11 for the left hand engine, where zones 4 and 5 are used specifically to quantify the inlet related components. Zones 6 and 7 capture the high frequency noise components in the immediate exhaust region; the low frequency mixing noise components are captured by zones 8 and 10, and 9 and 11. Note that zones 8 and 9 are available for both airframe and low frequency engine exhaust noise source quantification, the selection of which depends on aircraft high lift configuration and engine power setting (i.e., takeoff versus approach configuration). Jet/flap interaction effects will be present within zones 8 and 9, the extent of which will depend on the trailing edge jet exhaust configuration and physical extent, and power setting.

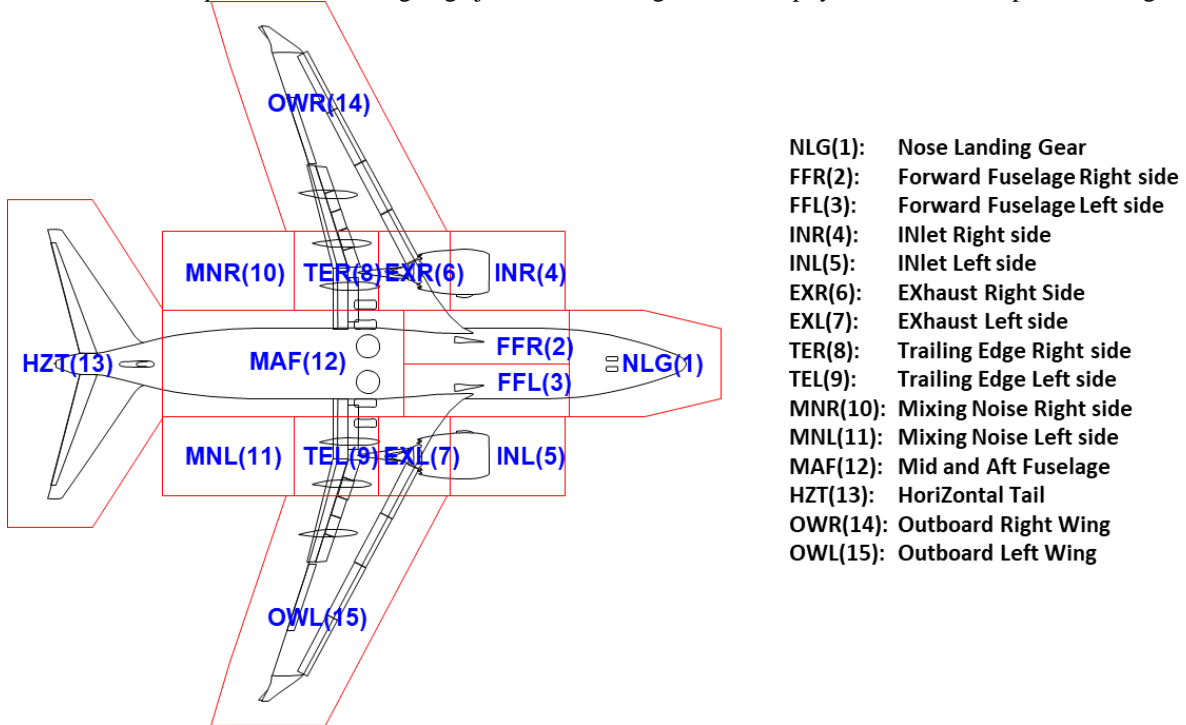


Fig. 7 Noise integration subregions.

The criticality of the use of the phased array for this study can be understood when considering single microphone noise measurements. It is well known that for modern commercial turbofan aircraft at takeoff conditions the total aircraft noise is dominated by the engine component. With the continued move to higher bypass ratio engines, noise levels at approach are found to be similar between the engine and airframe components. At higher engine power/takeoff conditions, the engines are the dominant noise sources, hence, the benefits of the inlet treatments are relatively easy to measure on a single microphone basis. However, for low takeoff powers and approach conditions, the inlet related noise levels can fall significantly below the levels of other (airframe and non-inlet related) noise sources and hence become unquantifiable on a single microphone basis. That is, the inlet noise levels have fallen below a limiting noise measurement floor for single microphone measurements. The phased array therefore provides a significant capability for being able to quantify the inlet related noise levels even when they fall to relatively low levels.

V. Phased Array Noise Subcomponent Characteristics

This section reviews sample phased array beamform map images and provides qualitative descriptions of the noise subcomponent breakdowns utilized in support of the analyses of Ref. 1. Examinations will be made at the engine blade passage frequency (BPF) and non-tonal frequencies at a forward angle for both takeoff and approach configurations, followed by similar examinations with the aircraft near overhead. This will highlight the fact that inlet directivity is primarily in the forward arc (see Ref. 1).

Figure 8 shows narrowband beamform maps at BPF for low power takeoff at a forward emission angle. The images are colored based on the noise levels within 8 dB of the peak level in a given map. The left and right hand images show the noise source for the hardwall and treated inlet configurations respectively. The hardwall inlet noise source is quite compact spatially, whereas the treated inlet noise distribution is of a more complex character. Based on examination of narrowband spectra, the overall reduction in tone level is on the order of several dB. That is, the level associated with the highest value in the hardwall inlet map is several dB higher than in the treated inlet map. Clearly absent from the maps is any indication of either exhaust noise or airframe noise related sources. This is not to say that they do not exist, but that they simply fall below the shown 8 dB display and/or phased array measurement dynamic range.

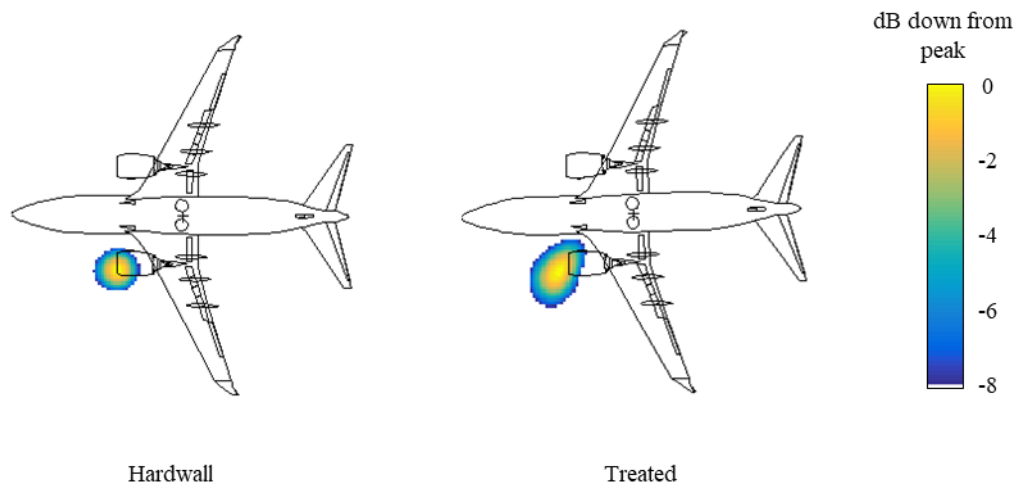


Fig. 8 Low power takeoff phased array images at 60 degree emission angle and at BPF.

Figure 9 shows narrowband beamform maps at a non-tonal high frequency for low power takeoff at a forward emission angle, namely at a frequency for which the inlet attenuation is largest. At this frequency the image is dominated completely by the inlet hardwall noise source. That is, all other sources (engine exhaust and airframe) are more than 8 dB below the levels shown. This source has a more distributed character than for the hardwall BPF image in Figure 8, similarly suggesting a more complex acoustic character. At the same frequency, the treated inlet noise sources consist instead of both an inlet and an exhaust noise source component, where the inlet associated levels are overall lower than at the exhaust (as a result of the inlet treatment noise reduction effect), and the airframe noise levels are more than 8 dB below these two noise sources (as inferred from their absence in the image).

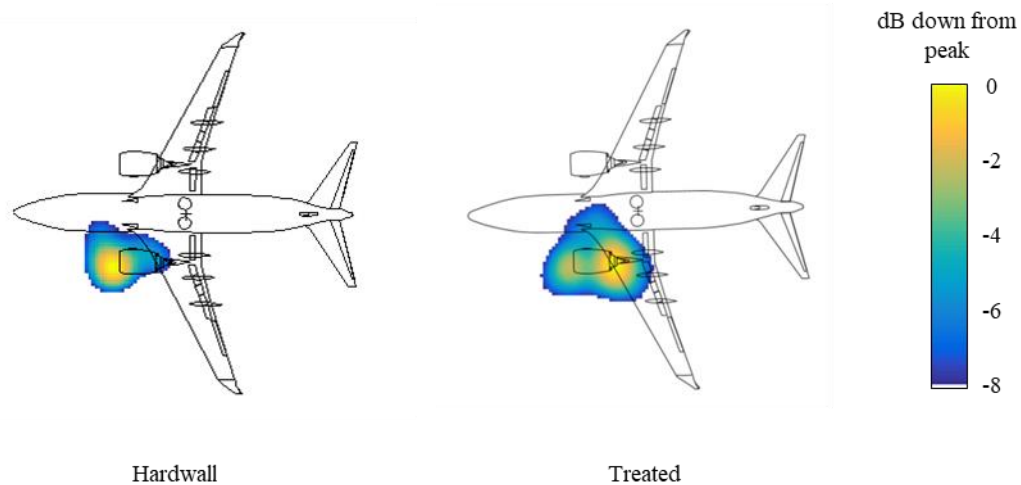


Fig. 9 Low power takeoff phased array images at 60 degree emission angle – broadband noise component at high frequency.

Figure 10 provides a qualitative spectral definition of the inlet, jet and airframe broadband noise sources (red, green and blue curves respectively) at forward angles for a low power takeoff configuration. These distributions are based qualitatively on measured data characteristics. The solid red and dashed red lines respectively represent the hardwall and treated inlet noise source levels versus frequency, the difference between the levels indicating the effect of the inlet liner on noise reduction. The noise components are dominated by jet noise over about half the bands, particularly at the lowest frequencies, and it is significantly higher than the airframe component levels over most bands. The hardwall inlet levels dominate at the higher frequencies. Note that the low frequency ends of the airframe and inlet related components do not extend to the lowest frequencies shown. This is a consequence of the levels of these components falling below the phased array measurement dynamic range.

The difference in level between the inlet related curves reaches a maximum at the frequency indicated by the right hand dashed vertical line. This corresponds to the frequency of the beamform noise maps shown in Figure 9. Included on the right side in the figure are insets based on the images in Figure 9 with the purpose of highlighting the relationship between what is seen in the phased array beamform noise maps and the noise component spectral components. Similarly, the insets to the left, which are based on Figure 8, relate to the narrowband tonal component at BPF, as suggested by the vertical red lines – exaggerated for clarity – associated with each of the two inlet related curves. The hardwall beamform map image (second from top left) corresponds to the right hand vertical red line representing the inlet tone, the peak of which is significantly higher than all other noise sources (hence, no other noise sources are evident in the map). The peak level in the treated case (left hand vertical red line) is noticeably lower than the hard wall peak tone level, but remains significantly above all other noise sources (8 dB or more) so that again no other noise sources are evident in the beamform map.

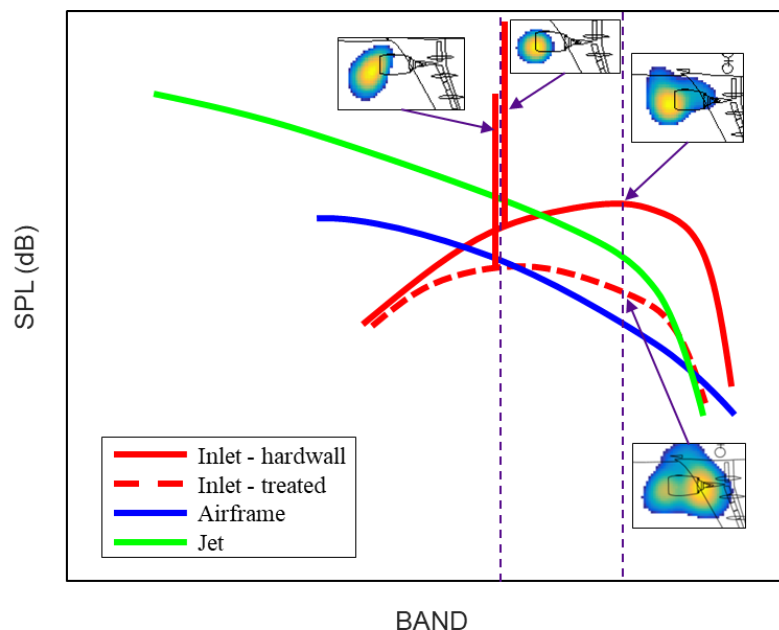


Fig. 10 Qualitative spectral distribution of broadband noise components at forward angles (low power takeoff).

At low engine power settings (largely at approach), the inlet broadband component levels will be relatively low, as will be the airframe noise component owing to a corresponding low flight velocity. At high takeoff power, both the inlet and airframe components will be at their highest levels (high engine setting and highest flight velocity). At low takeoff power, the inlet component will be significantly lower than at full takeoff power, whereas the aircraft velocity remains relatively high, which can lead to a significant lowering of inlet noise levels relative to the non-propulsive sources, hence, making them difficult to quantify on a single microphone basis.⁹ The phased array is therefore used to distinguish between and quantify these various noise source components.

⁹ The relative levels between the three components (inlet, jet, airframe) will vary depending on engine power setting, high lift system configuration and aircraft velocity. Also keep in mind that the high lift system deployment is different between the approach and takeoff conditions, hence, the airframe noise would largely be self-similar for the takeoff

Figure 11 shows narrowband beamform maps at BPF for approach at a forward emission angle. Of note, the aircraft velocity is significantly lower than for a takeoff condition, and the trailing edge flaps are deployed at 30 degrees. The leading edge slats are also further extended than at takeoff. The airframe noise spectral content will therefore be more extensive in nature for the approach condition. As seen at left in Figure 11, the hardwall inlet BPF tone is clearly evident, however, unlike the corresponding takeoff configuration image in Figure 8, additional noise sources are seen in Figure 11, including inlet noise from the left hand engine and exhaust and trailing edge noise from both engines. This means that these latter noise sources are within 8 dB of the inlet peak tone level (as compared to the takeoff inlet peak tone level being 8 dB or more above all other noise sources as described earlier). For the treated inlet (right hand image in Figure 11), the BPF tone is reduced, leading to even more noise sources falling within the 8 dB measurement range. As seen, the treated inlet noise level is actually significantly lower than the corresponding exhaust noise and mid-wing trailing edge noise sources. On a single microphone basis, this means that it is essentially impossible to quantify the treated inlet noise levels for this condition. The power of the phased array is that it can isolate and quantify the treated inlet component noise levels in the presence of these other higher level noise sources.

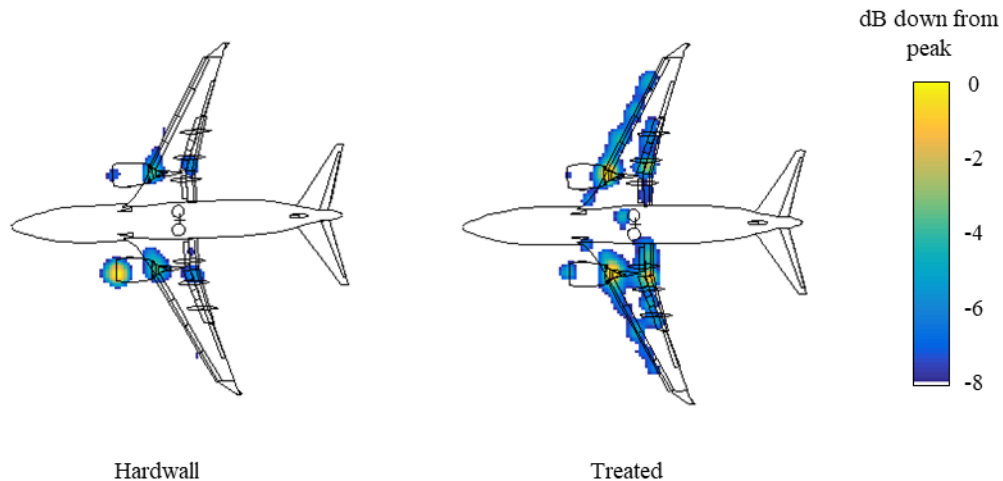


Fig. 11 Approach power phased array images at 60 degree emission angle and at BPF.

Figure 12 shows narrowband beamform maps at a non-tonal frequency for approach at a forward emission angle, namely at a frequency for which the inlet attenuation is largest. At this frequency the image is dominated completely by the inlet hardwall noise. At the same frequency, the treated inlet noise sources consist instead of both an inlet and an exhaust noise component, a right hand engine inlet component and several leading and trailing edge noise sources. This indicates that the hardwall inlet broadband component level is on the order of perhaps 8 dB to 12 dB above these latter noise sources, and that the broadband noise reduction is on the order of 4 dB.

configurations but would have a more varied energy content for the approach configuration owing to the added noise generating mechanisms (further extended flap and leading edge components). See Table 1.

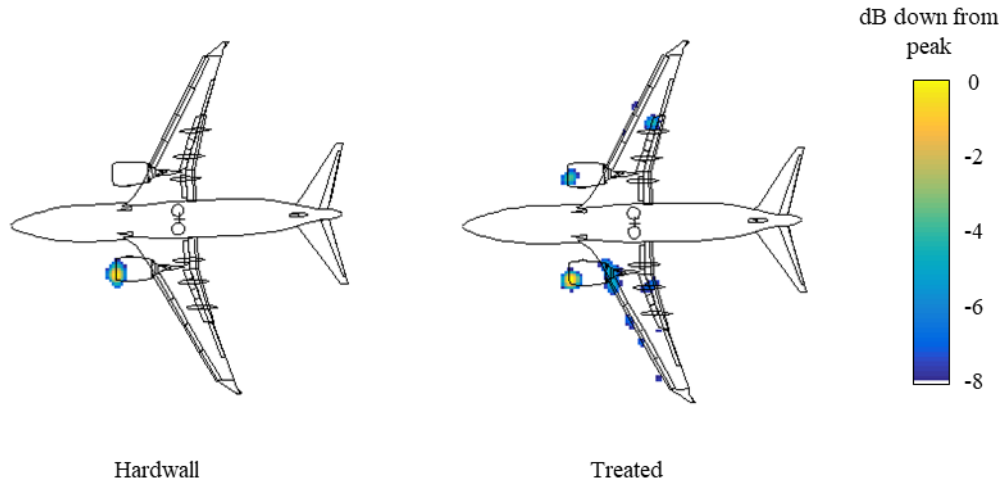


Fig. 12 Approach power phased array images at 60 degree emission angle – broadband noise component at high frequency.

Figure 13 provides a qualitative spectral definition of the broadband noise sources at forward angles for an approach configuration. Note how, as a result of the lower engine power setting, the jet noise component has been reduced significantly and now falls below the airframe component over all but the lowest frequencies. The inlet levels dominate at the higher frequencies. The difference in level between the hardwall and treated inlet curves reaches a maximum on the order of 4 dB at the frequency indicated by the right hand dashed vertical line. This corresponds to the frequency of the narrowband beamform noise maps shown in Figure 12. Insets based on the images are likewise included in Figure 13 to highlight the relationship between what is seen in the both the phased array beamform noise maps and the noise component spectral components (as described in the preceding paragraphs).

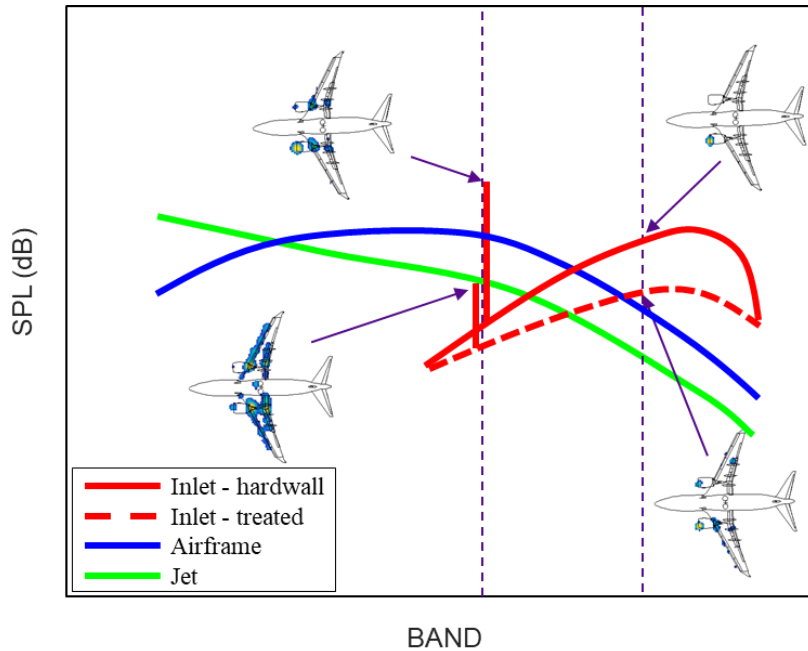


Fig. 13 Qualitative spectral distribution of broadband noise components at forward angles (approach power).

Figure 14 shows narrowband beamform maps at BPF for low power takeoff with the airplane near overhead (90 degree emission angle). The hardwall inlet noise source is fairly compact spatially, similar to what was seen in the corresponding image in Figure 8, but is broader in extent, extending over the inboard leading edge. The treated inlet noise distribution in Figure 14 shows that the exhaust region is the dominating noise source, with significantly lower inlet levels. The corresponding narrowband spectra (not shown) indicate a local peak in levels at BPF, indicating that the exhaust region energy is a result of inlet related tonal energy that has propagated aft and exited through the bypass duct. Additional energy is also seen inboard on the left hand side of the aircraft. Based on the 8 dB colorbar range, the differences in character of the images suggests an overall reduction in tone level on the order of a few dB.

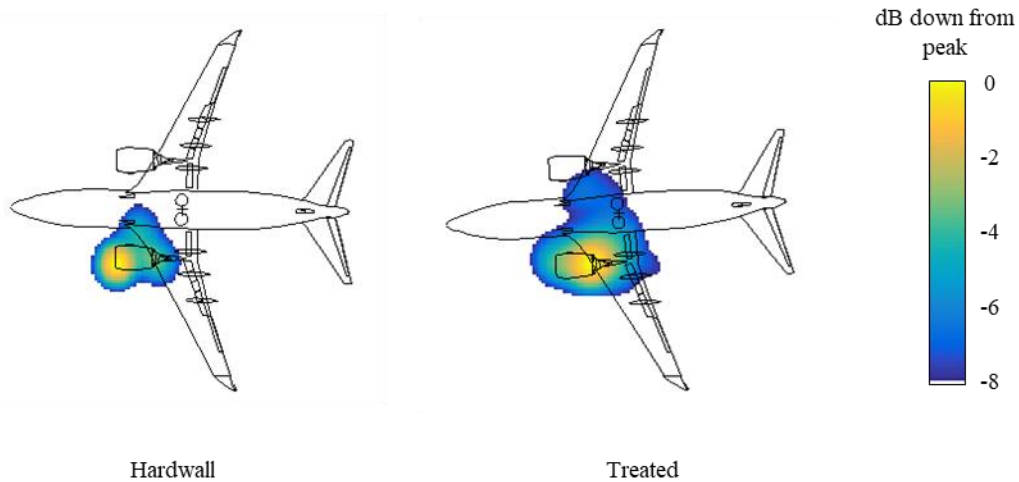


Fig. 14 Low power takeoff phased array images at 90 degree emission angle and at BPF.

Figure 15 provides a qualitative spectral definition of the broadband noise sources at forward angles for a low power takeoff configuration with the airplane near overhead (90 degree emission angle). At this angle and power setting, the engine related components are seen to generally dominate over all frequencies. The difference in level between the hardwall and treated curves is on the order of a few dB at the frequency indicated by the right hand dashed vertical line. This corresponds to the frequency of the narrowband beamform noise maps shown in Figure 14. Insets based on the images are likewise included in Figure 15.

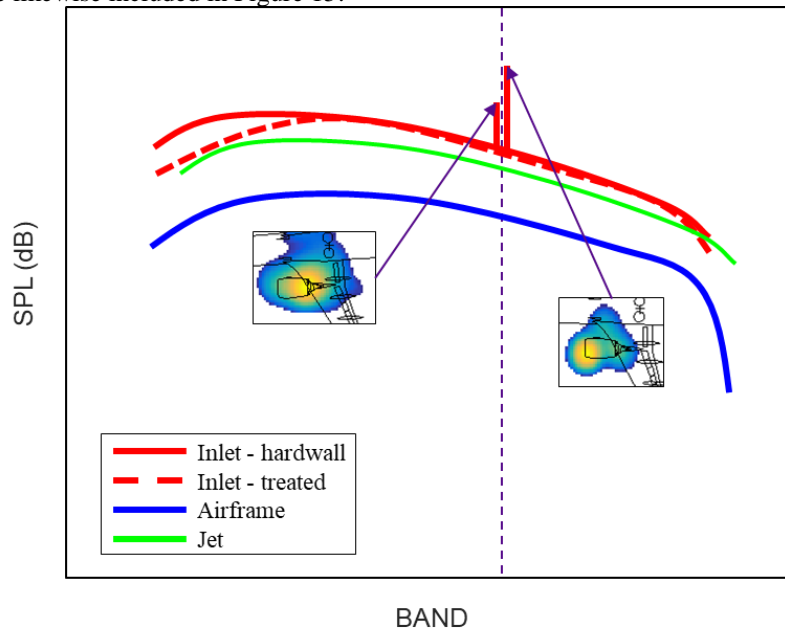


Fig. 15 Qualitative spectral distribution of BPF noise components at 90 degree emission angle (low power takeoff).

Figure 16 shows narrowband beamform maps at BPF for the approach configuration with the airplane near overhead (90 degree emission angle). The hardwall inlet noise source is clearly much lower in level than the exhaust noise source, again, significantly in contrast with the corresponding forward angle approach image in Figure 11, for which the inlet noise source largely dominates. This again highlights the propagation of the inlet related tonal noise aft through the bypass duct. The treated inlet noise distribution in Figure 16 shows that the inlet region noise is more than 8 dB below the exhaust region noise that dominates the peak levels. Considerably more airframe noise sources are evident in the image.¹⁰ In spite of being more evident in the image, the integration of the airframe noise associated energy remains lower than for the integrated engine components. The reduced inlet noise source level effects are a consequence of the directivity of the inlet noise source, which is maximum in the forward angles [see Ref. 1]. In concept, the exhaust noise levels could be used to quantify the inlet related tone levels owing to the aforementioned bypass duct sound propagation effect.

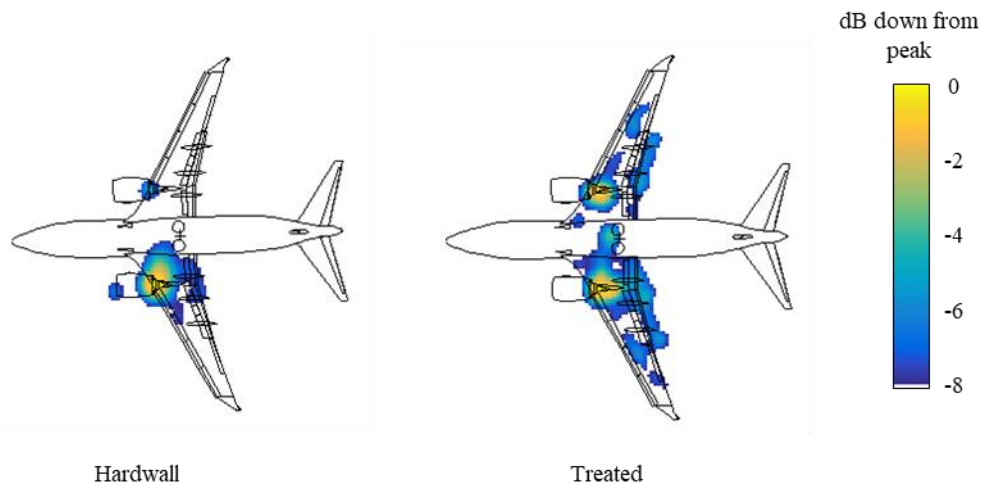


Fig. 16 Approach power phased array images at 90 degree emission angle and at BPF.

Figure 17 provides a qualitative spectral definition of the broadband noise sources for the approach configuration with the airplane near overhead. As suggested by the image, all subcomponents are similar in level, with the airframe noise component generally being the highest. Keeping in mind that the inlet and jet noise components are based on a single engine, the total inlet and jet levels would be 3 dB higher if the left hand engine was operating at the same thrust as the test engine, in which case, the airframe noise component would no longer be the overall dominant cumulative noise source. In Figure 17, the inlet related tone levels are instead indicated by green vertical lines in the figure, where the magnitude of the lines are based on levels inferred from the exhaust region tone levels and assumed to be representative of the inlet tone levels. Insets based on the images are likewise included in Figure 17. The inferred impact of the inlet liner on the tone levels propagating out of the exhaust duct is small, as would be expected.

¹⁰ The flight direction mismatch between the airframe noise sources and the airplane outline are a result of parallax owing to a flat beamforming grid having been used; the grid passes through the engine axes and accounts for aircraft pitch.

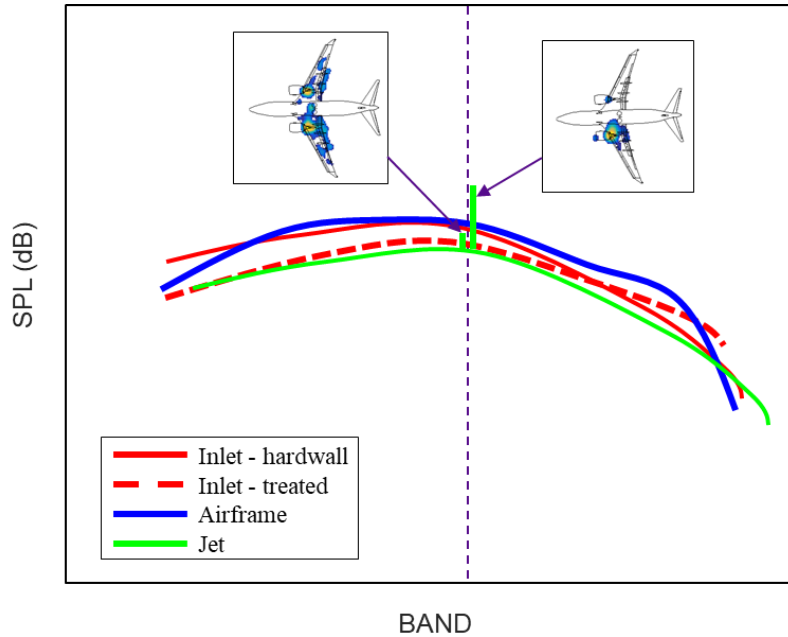


Fig. 17 Qualitative spectral distribution of BPF noise components at overhead angles (approach power, 90 degree emission angle).

VI. Summary

A description has been provided of the phased array analysis process used for separating out and quantifying the inlet noise component of the NASA advanced inlet liner tested as part of the Quiet Technology Demonstrator 3 flight test program, done in support of the work presented in Reference 1. A method was demonstrated for quantifying the usable frequency ranges of subarrays of the phased array system based on phased array map quality. Qualitative spectral definitions of the inlet, airframe and jet noise components were provided along with example phased array beamform maps.

Acknowledgments

L. Brusniak, J. W. Wong and E. H. Nesbitt would like to thank the entire NASA Langley team for sponsoring the flight test project. Additional thanks go to Wayne Wenneman, Jim Underbrink and Todd Schulz of the Boeing Aerodynamics/Noise/Propulsion laboratory for the successful phased array installation and acquisition of phased array data used in this study.

References

- [1] Wong, J. W., et al., "Flight Test Methodology for NASA Advanced Inlet Liner on 737MAX-7 Test Bed (Quiet Technology Demonstrator 3)," Abstract submitted for the 25th AIAA/CEAS Aeroacoustics Conference (Aeroacoustics 2019), 20-24 May, 2019, Delft, The Netherlands.
- [2] Brusniak, L., Underbrink, J.R. and Stoker, R. W., "Acoustic Imaging of Aircraft Noise Sources Using Large Aperture Phased Array," 12th AIAA/CEAS Aeroacoustics Conference (27th AIAA Aeroacoustics Conference), AIAA Paper 2006-2715, May 2006.
- [3] Underbrink, J., "Pletharrays for aeroacoustic phased array applications," International Journal of Aeroacoustics, Vol. 16, Issue 4-5, July 2017, pp. 202–229.
- [4] Howell, G. P., Bradley, A. J., et al., "De-Dopplerization and Acoustic Imaging of Aircraft Flyover Measurements," Journal of Sound and Vibration, 105 (1), pp. 151-167, 1986.
- [5] Dougherty, R. P., "Extensions of DAMAS and Benefits and Limitations of Deconvolution in Beamforming," AIAA Paper 2005-2961, 2005.
- [6] Brusniak, L., "DAMAS2 validation for flight test airframe noise measurements", 2nd Berlin Beamforming Conference, 19-20 February, 2008, (2008).
- [7] Lockard, D. P. and Bestul, K. A., "The Impact of Local Meteorological Conditions on Airframe Noise Flight Test Data," AIAA Paper 2018-2971, 2018.

[8] The Boeing Company, "Noise Source Decomposition System and Method Using an Adaptable Aperture Phased Array", United States Patent 9,213,078, Dec 15, 2015.